Parameter Extraction for 2-π Equivalent Circuit Model of RF CMOS Spiral Inductors*

Gao Wei and Yu Zhiping†

(Institute of Microelectronics, Tsinghua University, Beijing 100084, China)

Abstract: A novel parameter extraction method with rational functions is presented for the 2-π equivalent circuit model of RF CMOS spiral inductors. The final S-parameters simulated by the circuit model closely match experimental data. The extraction strategy is straightforward and can be easily implemented as a CAD tool to model spiral inductors. The resulting circuit models will be very useful for RF circuit designers.

Key words: 2-π; compact model; parameters extraction; RF CMOS; spiral inductors
EEACC: 2560B; 2570D
CLC number: TP211+.51 **Document code:** A **Article ID:** 0253-4177(2006)04-0667-07

1 Introduction

CMOS RFICs are now commonly used in wireless communications because of their low cost and easy integration. As passive components in RF ICs, spiral inductors[1] play a very important role in impedance matching, inductive source degeneration[2], LC-resonant tanks[3,4], and filters and baluns. However, due to the parasitic couplings and loss introduced by the conductive Si-substrate, the modeling of the spiral inductors has become a difficult task.

Compared with electromagnetic (EM) field solvers (e.g. HFSS) and partial-element-equivalent-circuit (PEEC)-based solvers[5] (e.g. ASITIC[6] and Momentum in ADS), a compact circuit model of the spiral inductors using lumped frequency-independent RLC elements would be more desirable for circuit simulations because of its advantage in speed and its inborn compatibility with SPICE.

There are two types of topologies for equivalent circuits of the spiral inductors: (1) the 1-π model[7~12], which is simple and has been successfully applied to the spiral inductors on an insulating substrate[8] but fails to capture the high frequency behavior (especially beyond the self resonant frequency, SRF); and (2) the 2-π model[13,14], which can model both the high-frequency behavior and the effects of a lossy substrate. The challenge in applying the 2-π model lies in the parameter extraction, which determines the final accuracy of the model. In Ref. [14], a comprehensive approach of parameter extraction using rational functions is proposed. However, the method is not straightforward. The scaling relationship $\xi(\omega)$ is not well determined and requires some manual manipulation, resulting in some uncertainty and randomness in the extracted parameter values. The method is therefore difficult to be implemented in CAD. In this paper, we propose an improved method that is step-by-step and easily realizable in CAD.

2 Rational function and two specific applications

2.1 Rational function

The general form of a rational function is written as

$$R(s) \equiv \frac{N_m(s)}{D_n(s)} \equiv \frac{a_0 + a_1 s + a_2 s^2 + \cdots + a_m s^m}{b_0 + b_1 s + b_2 s^2 + \cdots + b_n s^n} \tag{1}$$

where $N_m(s)$ and $D_n(s)$ are m- and n-order polynomials of variable s. There are $m + n + 2$ coefficients, $\{a_0, a_1, a_2, \cdots, a_m\}$ and $\{b_0, b_1, b_2, \cdots, b_n\}$, for which $a_m \neq 0$ and $b_n \neq 0$. Since one of $\{a_0, b_0, a_m, b_n\}$

---

* Project supported by the National High Technology Research and Development Program of China (No. 2004AA1Z11050)
† Corresponding author. Email: yuzhip@tsinghua.edu.cn
Received 9 October 2005, revised manuscript received 16 November 2005

can be assumed to be unity, there are only $m+n+1$ independent coefficients. For example, if $a_0 \neq 0$, one can normalize all the coefficients by dividing by a_0 so that a_0 is normalized to unity. In the following, we assume $a_0 = 1$.

Normally, $R(s)$ is expressed as a series of data points $\{R_1, R_2, \cdots, R_N\}$, measured at $\{s_1, s_2, \cdots, s_N\}$. Thus Equation (1) can be transformed into N linear equations for as and bs:

$$\begin{aligned} b_0 R_i + b_1 R_i s_i + b_2 R_i s_i^2 + \cdots + b_n R_i s_i^n &= 1 + a_1 s_i + a_2 s_i^2 + \cdots + a_m s_i^m, \\ i &= 1, 2, \cdots, N \end{aligned} \tag{2}$$

where $R_i = R(s_i)$. Usually $N > m+n+1$, so the above equations turn into an over-determined problem and can be solved as a standard linear least-square problem: $\min(v\ \|Ax - b\|)$, where $x = (a_1, \cdots, a_m, b_0, b_1, \cdots, b_n)^T \in R^{m+n+1}$ is a column vector for unknown coefficients and $b = (1, 1, \cdots, 1)^T \in R^N$ is a unity column vector. Thus,

$$A = \begin{bmatrix} -s_1 & -s_1^2 & \cdots & -s_1^m & R_1 & R_1 s_1 & R_1 s_1^2 & \cdots & R_1 s_1^n \\ -s_2 & -s_2^2 & \cdots & -s_2^m & R_2 & R_2 s_2 & R_2 s_2^2 & \cdots & R_2 s_2^n \\ \cdots & & & \cdots & \cdots & & \cdots & & \cdots \\ -s_N & -s_N^2 & \cdots & -s_N^m & R_N & R_N s_N & R_N s_N^2 & \cdots & R_N s_N^n \end{bmatrix} \tag{3}$$

$A \in R^{N(m+n+1)}$, and is expressed in Eq. (3).

2.2 Application for skin and proximity effects

Figure 1 (a) is used to model the skin and proximity effects[15]. Assuming $s = j\omega$, the impedance of the branch is

$$Z(s) = sL_s + R_s + \frac{sL_{sk} R_{sk}}{sL_{sk} + R_{sk}} \tag{4}$$

For $\omega = 0$, $Z(0) \equiv R_{DC} = R_s$. Then

$$\begin{aligned} \frac{Z(s) - Z(0)}{s} &= L_s + \frac{L_{sk} R_{sk}}{sL_{sk} + R_{sk}} \\ &= \frac{1 + \dfrac{L_s L_{sk}}{R_{sk}(L_s + L_{sk})} s}{\dfrac{1}{L_s + L_{sk}} + \dfrac{L_{sk}}{R_{sk}(L_s + L_{sk})} s} \end{aligned} \tag{5}$$

By evaluating the quantity $[Z(s) - Z(0)]/s$ at different frequencies $(\omega_1, \omega_2, \cdots, \omega_N)$ and fitting the results using the following rational function

$$\frac{1 + a_1 s}{b_0 + b_1 s} \tag{6}$$

and then by comparing Eqs. (5) and (6) with the extracted values of a_1, b_0, and b_1, the values of L_s, L_{sk}, and R_{sk} can be uniquely determined.

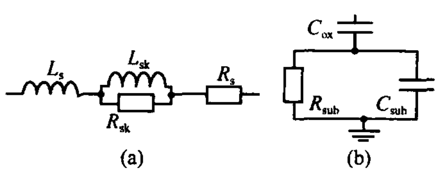

Fig. 1 (a) Skin effect model; (b) Oxide-substrate 3-element model

2.3 Application for the 3-element model of substrate loss

The 3-element model is commonly used to model the substrate loss as shown in Fig. 1(b). If the impedance for that branch is measured, then

$$\begin{aligned} Z(s) &= \frac{1}{sC_{ox}} + \frac{R_{sub}}{1 + sC_{sub} R_{sub}} \\ &= \frac{1 + s(C_{ox} + C_{sub}) R_{sub}}{sC_{ox} + s^2 C_{ox} C_{sub} R_{sub}} \end{aligned} \tag{7}$$

We fit the rational function

$$\frac{1 + a_1 s}{b_1 s + b_2 s^2} \tag{8}$$

to obtain a_1, b_1, and b_2, and thus the three elements C_{ox}, R_{sub}, and C_{sub} can be determined by comparing Eqs. (7) and (8).

3 Compact circuit model of spiral inductors

3.1 On-chip spiral inductors and the 1-π model

The on-chip spiral inductor and its basic 9-element 1-π circuit model are shown in Fig. 2. It is a 2-port device characterized by 2-port S-parameters (or other small signal parameters such as Y-parameters). For a linear passive network, $S_{12} = S_{21}$ (or $Y_{12} = Y_{21}$) due to its reciprocal nature. Hence there are only three independent complex parameters that characterize the device. The Y-parameters, for example, can be transformed into the following six real quantities (Note: The average of Y_{12} and Y_{21} is used because there are inevitable measurement errors between them):

$$\begin{cases} L_{11} \equiv \dfrac{\mathrm{Im}(1/Y_{11})}{\omega} \\ L_{22} \equiv \dfrac{\mathrm{Im}(1/Y_{22})}{\omega} \\ Q_{11} \equiv \dfrac{\mathrm{Im}(1/Y_{11})}{\mathrm{Re}(1/Y_{11})} = -\dfrac{\mathrm{Im}(Y_{11})}{\mathrm{Re}(Y_{11})} \\ Q_{22} \equiv \dfrac{\mathrm{Im}(1/Y_{22})}{\mathrm{Re}(1/Y_{22})} = -\dfrac{\mathrm{Im}(Y_{22})}{\mathrm{Re}(Y_{22})} \\ L_{eff} \equiv \dfrac{\mathrm{Im}(-1/\overline{Y_{21}})}{\omega} \\ R_{eff} \equiv \mathrm{Re}(-1/\overline{Y_{21}}) \end{cases} \tag{9}$$

where $\overline{Y_{21}} \equiv (Y_{12} + Y_{21})/2$.

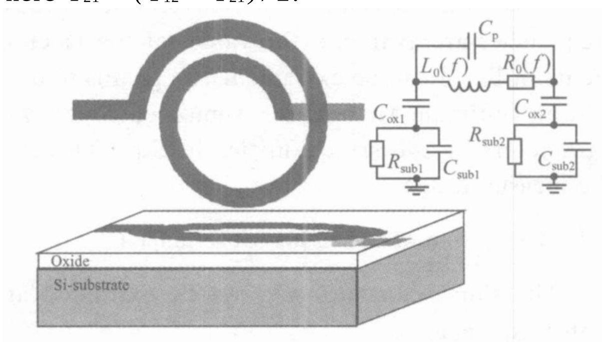

Fig. 2　On-chip spiral inductor and 1-π model

L_{11}, L_{22}, Q_{11}, and Q_{22} are the equivalent inductances and quality factors seen from Port1 and Port2 with the other port ac-shorted. L_{eff} and R_{eff} are the effective series inductance and resistance of the main path $(-\overline{Y_{21}})$. The DC values are:

$$\begin{cases} R_{DC} = R_{eff} \mid_{\omega\to 0} \\ L_{DC} = (L_{eff}, L_{11}, \text{or } L_{22}) \mid_{\omega\to 0} \end{cases} \tag{10}$$

where R_{DC} is the DC resistance, and L_{DC} is the inductance when $\omega\to 0$. The six quantities in Eq. (9) are mathematically equivalent to S- or Y-parameters, but they are more physically insightful and much easier to manage because they are all real numbers.

There are two sets of data for each quantity in Eq. (9), which represent the measured and simulated values, respectively. They are explicitly designated by a subscript "m" or "s"; for example, $L_{11,m}$ or $L_{11,s}$, and $Q_{11,m}$ or $Q_{11,s}$. The modeling goal is to let simulated values ("s") of all the six quantities be as close to the measured values ("m") as possible.

3.2　From the 1-π model to the 18-element 2-π model

The simple 1-π topology shown in Fig. 3(a) has serious deficiencies for a lossy substrate, as in CMOS RFICs. In Eq. (9), the quantity R_{eff} needs to be treated carefully. The measurements show that it equals to the DC resistance at first and then rises with frequency due to the skin and proximity effects. But after it reaches a maximum at $f_{skin,max}$ (Fig. 5), it begins to drop until reaching a negative value on the order $10^{-2} \sim 10^{-3}\Omega$ when the frequency is sufficiently high. This phenomenon is due to distributed substrate parasitics which override the skin and proximity effects, and can only be explained by a 2-π topology.

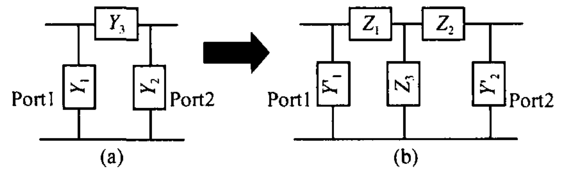

Fig. 3　Topology of 1-π (a) and 2-π (b) models

Figure 3(b) is a block diagram for the 2-π model, without the shunt capacitor C_p. Figure 4 is our 18-element 2-π model, refined from Ref. [13] with redundant elements removed. According to

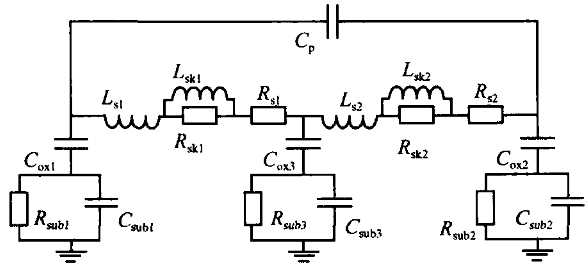

Fig. 4　18-element 2-π circuit model

Fig. 3(b), with a third grounded branch Z_3 added, the distributed effects of the substrate parasitics can be compensated by:

$$R_{eff} = \mathrm{Re}(Z_1 + Z_2 + Z_1 Z_2 / Z_3) \tag{11}$$

Assuming $Z_1 \approx R_{s1} + j\omega L_{s1}$, $Z_2 \approx R_{s2} + j\omega L_{s2}$ and $Z_3 \approx R_{sub3} + 1/j\omega C_{ox3}$, then

$$R_{eff} \approx \mathrm{Re}\left[(R_{s1} + j\omega L_{s1}) + (R_{s2} + j\omega L_{s2}) + \frac{(R_{s1} + j\omega L_{s1})(R_{s2} + j\omega L_{s2})}{R_{sub3} + 1/j\omega C_{ox3}}\right] \tag{12}$$

At high frequencies, we assume roughly that $R_{s1} \ll \omega L_{s1}$, $R_{s2} \ll \omega L_{s2}$, and $R_{sub3} \gg 1/(\omega C_{ox3})$, so

$$R_{eff} \approx R_{s1} + R_{s2} - \omega^2 L_{s1} L_{s2} / R_{sub3} \tag{13}$$

Thus R_{eff} can become negative at high enough frequencies due to the negative term that is $\propto \omega^2$. (Note: negative R_{eff} does not imply that the passivity of the model has been violated, because it is only an effective quantity with the unit of Ω and not a real resistance as defined from $-\overline{Y_{21}}$.) On the contrary, the 1-π model only provides a positive value of R_{eff} regardless of frequency because the "Y_3" box in Fig. 3(a) must be passive.

Figure 5 shows both the measured ("m") and simulated ("s") values using our 2-π model for R_{eff} and L_{eff} of a 4.5-turn spiral inductor fabricated in the TSMC 0.25μm process. The simulated results using the 1-π model provided by the foundry are also plotted and identified by the suffix "TSMC_1-π". This shows that the 1-π model gives inaccurate values for both R_{eff} and L_{eff} at high frequencies compared to the measured data. It predicts a high-Q parallel-tank resonating at about 13GHz and the sign of R_{eff} is always positive. On the contrary, the simulated results of the 2-π model are accurate at least up to the resonant frequency (about 15GHz as shown in Fig. 5).

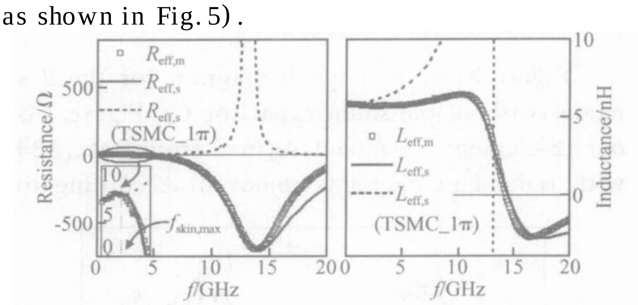

Fig. 5 R_{eff} and L_{eff} fabricated in a 4.5-turn inductor fabricated in TSMC 0.25μm process

3.3 Skin and proximity effects in the 2-π model

In order to model the skin and proximity effects, the single inductor $L_0(f)$ and resistor $R_0(f)$ in Fig. 2 must be frequency-dependent and not compatible with SPICE. Therefore two branches (L_{sk} and R_{sk}) are added in Fig. 4. Assuming the two halves of the main path are identical: $Z_1 \equiv Z_2$, the number of the independent elements of the circuit can be reduced to 14.

The effect of eddy-currents in the substrate is not included in this paper because the current RF CMOS process normally uses a lightly-doped Si-substrate ($\rho_{si} \approx 1 \sim 10\Omega \cdot cm$), in which eddy current effect is negligible.

3.4 Limitations of the 2-π model

The 2-π model has its own limitations at high frequencies: it is valid up to the self resonant-frequency (SRF). Beyond SRF, the spiral presents capacitive properties and cannot be used as an inductor any more. Thus the above upper limitation of the model is still acceptable for most circuit applications since SRF sets the applicable limit of spiral inductors. Moreover, the six quantities in Eq. (9) lose their physical meaning beyond SRF; and thus fitting error will be larger beyond SRF.

Seen from the two ports, SRF is defined as

$$\begin{cases} SRF_{11} \equiv \omega/2\pi \,|_{L_{11}=0} \\ SRF_{22} \equiv \omega/2\pi \,|_{L_{22}=0} \end{cases} \tag{14}$$

4 Parameter extraction in the 2-π model

When the measured S-parameters at various frequencies are available, the values of the 18 elements in Fig. 4 can be extracted. The goal is to obtain an optimum fit between simulated S- or Y-parameters or the six quantities in Eq. (9) with the measured data.

4.1 Extraction of the shunt capacitance C_p

The shunt capacitor C_p can be extracted at high frequencies as

$$C_p = \left.\frac{\mathrm{Im}(-\overline{Y}_{21,m})}{\omega}\right|_{\omega\to\infty} \tag{15}$$

The term "high frequency" is not well defined, and the measured data do not show an asymptotic constant, even when the frequency is kept increasing. Nevertheless, in order to perform the following extraction, C_p must be assigned a value. We evaluate Eq. (15) at the maximum measuring frequency and then determine C_p. Thus we can define

$$Z'_{eff,m} \equiv \frac{1}{-\overline{Y}_{21,m} - j\omega C_p} \tag{16}$$

4.2 Extraction of elements in Z_1 and Z_2

Since $Z_1 \equiv Z_2$ as shown in Fig. 3(b), each impedance is

$$Z_{1,m} = Z_{1,m} \approx Z'_{eff,m}/2, \quad f < f_{skin,max} \tag{17}$$

The above approximate equality holds only before $R_{eff,m}$ reaches its maximum: $f < f_{skin,max}$ as depicted in Fig. 5, when the shunt effect of Z_3 can be neglected. After $f_{skin,max}$, the skin and proximity effects on $R_{eff,m}$ (also $L_{eff,m}$) will be overridden by the capacitive substrate parasitics of Z_3 as explained in Section 3.2. We define:

$$f_{skin,max} \equiv \omega/2\pi \,|_{R_{eff,m}=\max(R_{eff,m})} \tag{18}$$

Thus the method described in Section 2.2 can be performed with the impedance of the LHS term of Eq. (4) already known, and the values of $L_{s1,2}$,

$R_{s1,2}$, $L_{sk1,2}$, and $R_{sk1,2}$ can be determined.

4.3 Extraction of elements in Z_3

When the elements in Z_1 and Z_2 are extracted, the impedance of Z_3 shown in Fig. 3(b) can be calculated as

$$Z_{1,s} = Z_{2,s} = R_{s1} + j\omega L_{s1} + \frac{R_{sk1}\, j\omega L_{sk1}}{R_{sk1} + j\omega L_{sk1}}$$

$$Z_{3,m} = \frac{(Z_{1,s})^2}{Z'_{eff,m} - 2Z_{1,s}} \tag{19}$$

where the simulated impedances $Z_{1,s}$ and $Z_{2,s}$ are evaluated at the measuring frequencies $\{\omega_1, \omega_2, \cdots, \omega_N\}$. Thus, with the impedance of the LHS term of Eq. (7) known, the method of Section 2.3 can be performed to determine C_{ox3}, R_{sub3}, and C_{sub3}.

4.4 Extraction of elements in Y'_1 and Y'_2

After the elements in Z_1, Z_2, and Z_3 are extracted, we can calculate Y'_1 and Y'_2 as shown in Fig. 3(b). Let

$$\begin{cases} Z_{3,s} = \dfrac{1}{j\omega C_{ox3}} + \dfrac{R_{sub3}}{1 + j\omega C_{sub3} R_{sub3}} \\ Y'_{1,m} = Y_{11,m} - \left(\dfrac{Z_{1,s} Z_{3,s}}{Z_{1,s} + Z_{3,s}} + Z_{1,s}\right)^{-1} - j\omega C_p \\ Y'_{2,m} = Y_{22,m} - \left(\dfrac{Z_{2,s} Z_{3,s}}{Z_{2,s} + Z_{3,s}} + Z_{2,s}\right)^{-1} - j\omega C_p \end{cases} \tag{20}$$

Thus the impedances $1/Y'_{1,m}$ and $1/Y'_{2,m}$ can be calculated, and the method described in Section 2.3 can be applied again to determine the values of $\{C_{ox1}, R_{sub1}, C_{sub1}\}$ and $\{C_{ox2}, R_{sub2}, C_{sub2}\}$, respectively.

Now the values of all 18 elements in Fig. 4 have been extracted.

5 Experimental validation

The measured data correspond to three inductors fabricated in Chartered Semiconductor's 0.18μm RF CMOS Cu-top 6-metal process. The layout parameters are shown in Table 1, covering turns $n = 1, 5, 7$ and the DC inductance $L_{DC} = 0.5$, 3.8, 11.3nH. The extracted values of circuit elements are also shown in the table. Figures 6～9 show the six quantities defined in Eq. (9). The *S*-parameters of only one inductor (D2) are plotted in Fig. 10 in order not to crowd the figure. The figure shows that the circuit model is very accurate up to the inductor's SRF (with max error less than 1%) provided that the parameters are properly extracted using our method. Beyond SRF, the circuit model presents more errors, but the trends are still correct.

Table 1　Parameter extraction results of three inductors fabricated in 0.18μm RF CMOS process

Device		D1	D2	D3
Layout parameter1)	n	1	5	7
	r/μm	50	34.5	50
	w/μm	12	6	12
	s/μm	1.8	1.8	1.8
DC value	R_{DC}/Ω	0.7	3.1	3.4
	L_{DC}/nH	0.5	3.8	11.3
Circuit element	C_p/fF	2.2	13.0	38.2
	$L_{s1,2}$/nH	0.246/0.246	1.81/1.81	5.25/5.25
	$L_{sk1,2}$/nH	0.104/0.104	0.091/0.091	0.305/0.305
	$R_{s1,2}$/Ω	0.375/0.375	1.55/1.55	1.68/1.68
	$R_{sk1,2}$/Ω	0.408/0.408	1.69/1.69	1.82/1.82
	$C_{ox1,2,3}$/fF	69.8/50.6/23.9	48.0/40.3/86.7	128/93.5/367
	$C_{sub1,2,3}$/fF	13.7/12.5/1.27	31.7/16.8/2.31	64.7/26.5/45.6
	$R_{sub1,2,3}$/Ω	563/714/496	250/367/415	75.4/214/152

1) n: turn, r: inner radius, w: metal width, s: metal spacing.

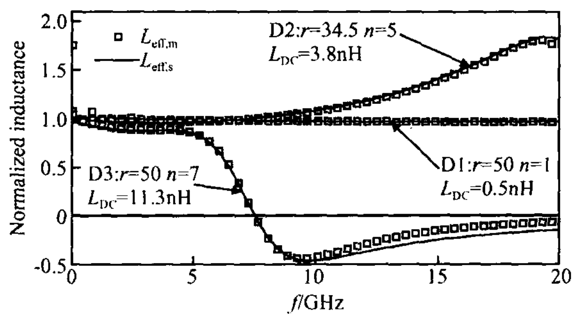

Fig. 6　Measured and simulated effective series inductances L_{eff} of three inductors normalized to their DC inductances

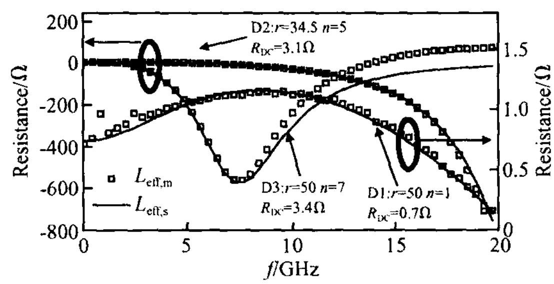

Fig. 7　Measured and simulated effective series resistances R_{eff} of three inductors

6 Conclusion

The 1-π equivalent circuit model[7,12] is not adequate for RF CMOS spiral inductors, but the 2-π topology is good for most applications[13,14]. The

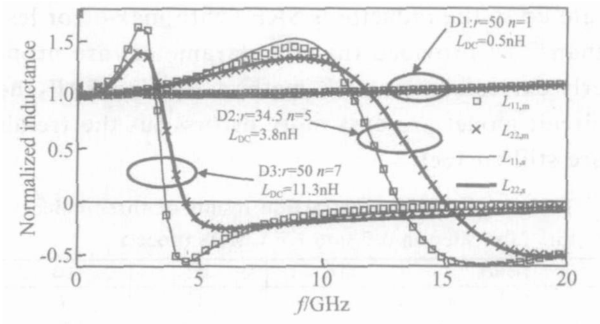

Fig. 8 Measured and simulated equivalent inductance L_{11} and L_{22} of three inductors normalized to their DC inductances

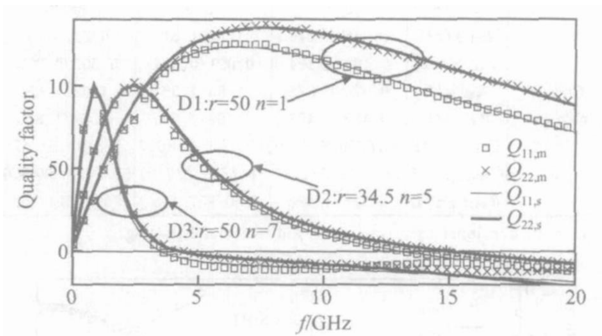

Fig. 9 Measured and simulated quality factors Q_{11} and Q_{22}

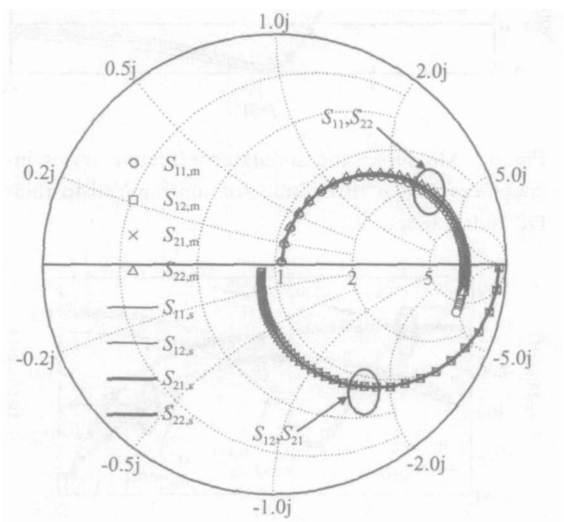

Fig. 10 Measured and simulated S-parameters of a 5-turn inductor (D2)

compact circuit model used in this paper is a refined version of the 2-π topology from Ref. [13] with redundant elements removed. The values of all 18 elements in our circuit model can be extracted step-by-step. The methodology of parameter extraction described in this paper is more straightforward and much more easily implemented as a CAD tool compared to the heuristic work[14].

The accuracy of the proposed parameter extraction method for the 2-π model of Fig. 4 is very good and has been verified by comparison to several industrial samples. The resulting circuit model is very useful for RF circuit designers.

Acknowledgment The experimental data from Chartered Semiconductor in Singapore is greatly appreciated. The close collaboration with Cadence in San Jose, USA plays a critical role in this work, and the authors are grateful to the team led by Dr. Ping Chen of Cadence.

References

[1] Burghartz J N, Rejaei B. On the design of RF spiral inductors on silicon. IEEE Trans Electron Devices, 2003, 50(3): 718

[2] Yao Fei, Cheng Buwen. Design of 1GHz 0.5μm CMOS low noise amplifier. Chinese Journal of Semiconductors, 2004, 25(10): 1291 (in Chinese) [姚飞, 成步文. 1GHz 0.5μm CMOS 低噪声放大器的设计. 半导体学报, 2004, 25(10): 1291]

[3] Chi Baoyong, Shi Bingxue, Wang Zhihua. A 2.4GHz CMOS monolithic transceiver front-end for IEEE 802.11b wireless LAN applications. Chinese Journal of Semiconductors, 2002, 23(2): 1731

[4] Yi Xiaofeng, Fang Han, Yang Yujia, et al. A 2.4GHz quadrature output frequency synthesizer. Chinese Journal of Semiconductors, 2005, 26(10): 1910

[5] Li Fuhua, Zhao Jixiang, Li Zhengfan. Modeling for spiral inductors on-chip with partial element equivalent circuit method. Chinese Journal of Semiconductors, 2005, 26(4): 770 (in Chinese) [李富华, 赵吉祥, 李征帆. 基于 PEEC 方法的片内螺旋电感建模. 半导体学报, 2005, 26(4): 770]

[6] Niknejad A M, Meyer R G. Analysis, design, and optimization of spiral inductors and transformers for Si RF ICs. IEEE J Solid-State Circuits, 1998, 33(10): 1470

[7] Yue C P, Wong S S. Physical modeling of spiral inductors on silicon. IEEE Trans Electron Devices, 2000, 47(3): 560

[8] Pieters P, Vaesen K, Brebels S, et al, Accurate modeling of high-Q spiral inductors in thin-film multilayer technology for wireless telecommunication applications. IEEE Trans Microw Theory Tech, 2001, 49(4): 589

[9] Scuderi A, Biondi T, Ragonese E, et al. A lumped scalable model for silicon integrated spiral inductors. IEEE Trans Circuits Syst I, 2004, 51(6): 1203

[10] Wang Yanfeng, Huang Qing'an, Liao Xiaoping. Parameters extraction methods of an RF spiral inductor. Chinese Journal of Semiconductors, 2005, 26(8): 1591 (in Chinese) [王彦丰, 黄庆安, 廖小平. RF 螺旋电感参数的提取方法. 半导体学报, 2005, 26(8): 1591]

[11] Lin Min, Li Yongming, Chen Hongyi. An optimization technique for planar spiral inductor based on the inductor's physical model and genetic algorithm. Chinese Journal of Semiconductors, 2001, 22(7): 897 (in Chinese) [林敏, 李永明, 陈弘毅. 一种基于物理模型与遗传算法的平面螺旋电感的

优化技术. 半导体学报,2001,22(7):897]
[12] Wang Tao, Wang Yong, Chen Kangsheng. A fast optimizing technique for planar spiral inductors based on binary search algorithm. Chinese Journal of Semiconductors, 2003, 24(9):999(in Chinese) [王涛,王勇,陈抗生. 一种基于二分搜索法的平面螺旋电感的快速优化技术. 半导体学报, 2003, 24(9):999]
[13] Cao Y, Groves R A, Huang X, et al. Frequency-independent equivalent-circuit model for on-chip spiral inductors. IEEE J Solid-State Circuits, 2003, 38(3):419
[14] Watson A C, Melendy D, Francis P, et al. A comprehensive compact-modeling methodology for spiral inductors in silicon-based RFICs. IEEE Trans Microw Theory Tech, 2004, 52(3):849
[15] Chao C J, Wong S C, Kao C H, et al. Characterization and modeling of on-chip spiral inductors for Si RFICs. IEEE Trans Semicond Manufact, 2002, 15(1):19

射频 CMOS 平面螺旋电感 2-π 等效电路模型参数的提取 *

高　巍　余志平†

(清华大学微电子学研究所, 北京　100084)

摘要: 从有理分式拟合方法出发,提出了用于射频 CMOS 平面螺旋电感 2-π 等效电路模型参数提取的新方法. 通过比较提参后等效电路给出的 S 参数和实验测量的 S 参数,证明该方法的精度很高. 此外,提参的策略非常直接,因此容易在 CAD 里面编程实现. 提参得到的等效电路模型对于射频电路设计者来说也是非常有用的.

关键词: 2-π; 等效电路模型; 参数提取; 射频 CMOS 电路; 平面螺旋电感
EEACC: 2560B; 2570D
中图分类号: TP211⁺.51　**文献标识码**: A　**文章编号**: 0253-4177(2006)04-0667-07

* 国家高技术研究发展计划资助项目(批准号:2004AA1Z11050)
† 通信作者. Email: yuzhip@tsinghua.edu.cn
2005-10-09 收到, 2005-11-16 定稿